ARTICLES

Journal of Semiconductors
(2019) 40, 062005
doi: 10.1088/1674-4926/40/6/062005

Substrates and interlayer coupling effects on $Mo_{1-x}W_xSe_2$ alloys

Fang Liang[1], Hejun Xu[1], Zuoyuan Dong[1], Yafeng Xie[2], Chen Luo[1], Yin Xia[1], Jian Zhang[1], Jun Wang[2], and Xing Wu[1, †]

[1]Shanghai Key Laboratory of Multidimensional Information Processing, Department of Electronic Engineering, East China Normal University, Shanghai 200241, China

[2]Laboratory of Micro-Nano Photonic and Optoelectronic Materials and Devices, Key Laboratory of Materials for High-Power Laser, Shanghai Institute of Optics and Fine Mechanics, Chinese Academy of Sciences, Shanghai 201800, China

Abstract: Two-dimensional (2D) transition metal dichalcogenides alloys are potential materials in the application of photodetectors over a wide spectral range due to their composition-dependent bandgaps. The study of bandgap engineering is important for the application of 2D materials in devices. Here, we grow the $Mo_{1-x}W_xSe_2$ alloys on mica, sapphire and SiO_2/Si substrates by chemical vapor deposition (CVD) method. $Mo_{1-x}W_xSe_2$ alloys are grown on the mica substrates by CVD method for the first time. Photoluminescence (PL) spectroscopy is used to investigate the effects of substrates and interlayer coupling force on the optical bandgaps of as-grown $Mo_{1-x}W_xSe_2$ alloys. We find that the substrates used in this work have an ignorable effect on the optical bandgaps of as-grown $Mo_{1-x}W_xSe_2$. The interlayer coupling effect on the optical bandgaps of as-grown $Mo_{1-x}W_xSe_2$ is larger than the substrates effect. These findings provide a new way for the future study of the growth and physical properties of 2D alloy materials.

Key words: $Mo_{1-x}W_xSe_2$; substrates; two-dimensional materials; bandgaps; photoluminescence

Citation: F Liang, H J Xu, Z Y Dong, Y F Xie, C Luo, Y Xia, J Zhang, J Wang, and X Wu, Substrates and interlayer coupling effects on $Mo_{1-x}W_xSe_2$ alloys[J]. *J. Semicond.*, 2019, 40(6), 062005. http://doi.org/10.1088/1674-4926/40/6/062005

1. Introduction

Two-dimensional (2D) materials, such as black phosphorus (BP)[1], topological insulators[2], transition metal dichalcogenides (TMDs) materials[3–8], have become popular research topics since graphene was discovered by Novoselov *et al.* in 2004[9]. TMD-layered materials with graphene-like structures have potential applications in digital electronics, optoelectronics devices and thermoelectrical fields due to their outstanding electronic, optical, and thermal properties. TMD-layered materials, such as $MoSe_2$ and WSe_2, have strong light-matter interactions and broad-band light absorption, and are promising materials for use in constructing various photodetectors[10, 11]. However, several works have reported that binary TMD-layered materials may introduce defects, such as chalcogen vacancies. Unfortunately, these defects usually serve as localized deep-level defect states[12–14], which have an enormous influence on the photoresponse of photodetectors. Yao *et al.*[13] have reported that localized deep-level defect states can be effectively suppressed by alloys.

Both theoretical and experimental studies[15–21] indicate that layered-TMD alloys have bandgaps that can be tuned by adjusting the composition of the corresponding atoms. Moreover, the thermodynamic properties of layered-TMD alloys are theoretically more stable than their binary counterparts. Thus, layered-TMD alloys, which have composition-dependent bandgaps, are able to extend the use of 2D materials in photodetectors over a wide spectral range. However, currently, only several TMD ternary alloys, such as $MoSe_{2(1-x)}S_{2x}$[20,22], $WS_{2x}Se_{2-2x}$[23], $Mo_{1-x}W_xSe_2$[24–28], and $Mo_{1-x}W_xSe_2$[17, 29, 30], have been studied experimentally. There is still no systematic study on the $Mo_{1-x}W_xSe_2$ alloys due to the difficulty of their synthesis.

In this work, the $Mo_{1-x}W_xSe_2$ alloys are synthesized on mica, sapphire and SiO_2/Si substrates by the chemical vapor deposition (CVD) method. The $Mo_{1-x}W_xSe_2$ alloys are first synthesized on the mica substrates by the CVD method. The effects of substrates and interlayer coupling force on the as-grown $Mo_{1-x}W_xSe_2$ alloys are then investigated by an atomic force microscope (AFM), Raman spectroscopy and photoluminescence (PL) spectroscopy. The results show that the as-used substrates have negligible effects on the bandgaps of the $Mo_{1-x}W_xSe_2$ alloys, while the interlayer coupling effect on the optical bandgaps of $Mo_{1-x}W_xSe_2$ alloys is greater than the substrates.

2. Result and discussion

The $Mo_{1-x}W_xSe_2$ alloys are prepared on different substrates and are synthesized using the CVD method. The details are introduced in the method section. A schematic of the CVD growing setup is shown in Fig. 1(a). The size of $Mo_{1-x}W_xSe_2$ alloys on SiO_2/Si substrates as a function of the growing time is illustrated in Fig. 1(b), which reveals that the size of $Mo_{1-x}W_xSe_2$ alloys increases with the incremental growth time within 25 min. Raman spectroscopy is a fast and accurate but nondestructive tool to study material structures and properties[31, 32]. The Raman spectra of $Mo_{1-x}W_xSe_2$ alloys on different substrates are shown in Fig. 1(c). The prominent peaks occurring around 241 cm^{-1} are the A_{1g} Raman modes of as-grown $Mo_{1-x}W_xSe_2$ alloys. The inset in Fig. 1(c) shows the weak $E_{2g}{}^1$ peaks of $Mo_{1-x}W_xSe_2$ alloys on different substrates. The

Correspondence to: X Wu, xwu@ee.ecnu.edu.cn
Received 12 JANUARY 2019; Revised 27 FEBRUARY 2019.

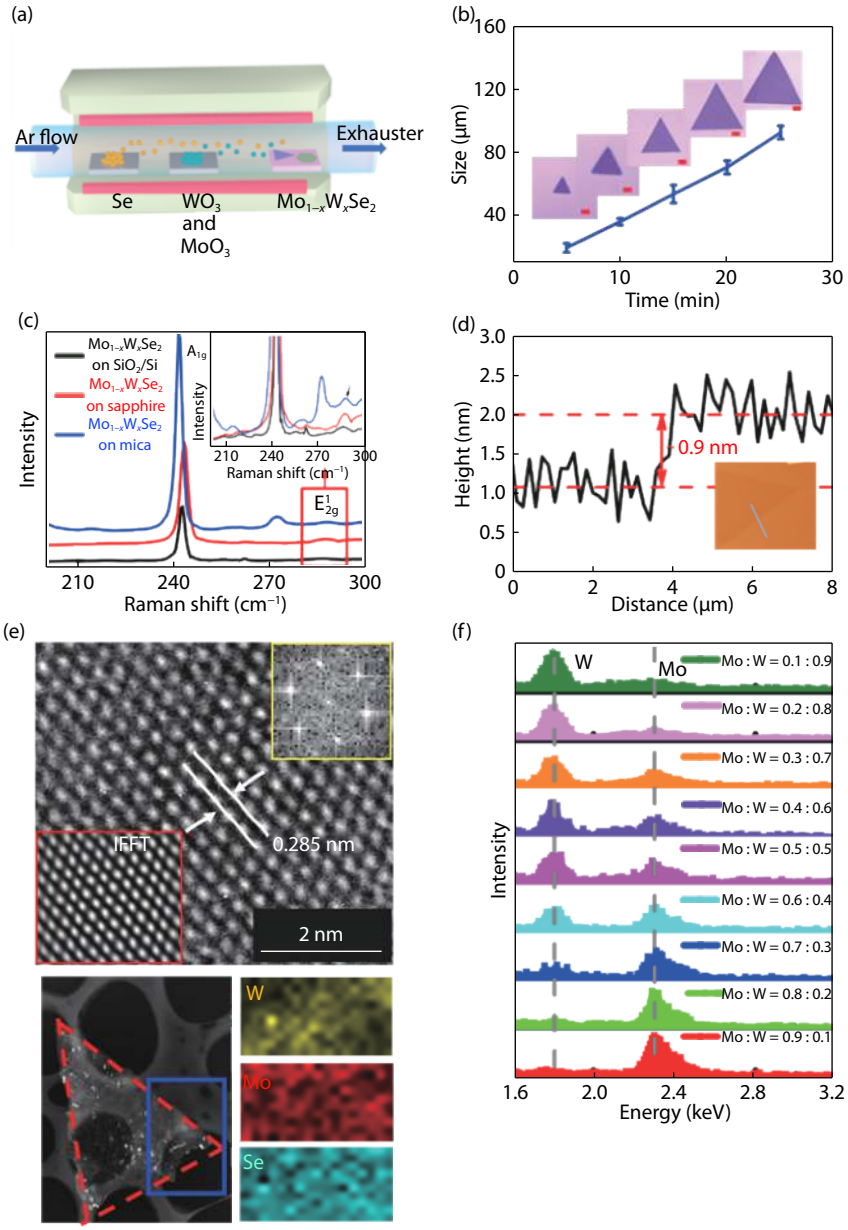

Fig. 1. (Color online) The synthesis and characterization of $Mo_{1-x}W_xSe_2$ alloys. (a) Schematic of the chemical vapor deposition setup for $Mo_{1-x}W_xSe_2$ alloys. (b) The time-dependent size curve of the $Mo_{1-x}W_xSe_2$ alloys grown by CVD on SiO_2/Si. The insets show the triangle shape of the as-grown $Mo_{1-x}W_xSe_2$ alloys with different size. The scale bar is 5 μm. (c) The Raman spectra of as-grown $Mo_{1-x}W_xSe_2$ alloys on different substrates. (d) AFM image of the as-grown $Mo_{1-x}W_xSe_2$ alloys. The AFM result shows that the thickness of the as-grown $Mo_{1-x}W_xSe_2$ is about 0.9 nm. (e) TEM result of as-grown $Mo_{1-x}W_xSe_2$ alloys. The bottom left shows the low-resolution TEM image and the bottom right shows the Mo, W, Se element mapping images of as-grown $Mo_{1-x}W_xSe_2$ alloys. The top view shows the HRTEM image of as-grown $Mo_{1-x}W_xSe_2$ alloys, the scale bar is 2 nm. The distance along the crystal plane (100) is 0.285 nm. The top right-hand inset of HRTEM image shows the corresponding selected area electron diffraction pattern (SAED), which demonstrates the as-grown $Mo_{1-x}W_xSe_2$ samples have the hexagon structure. The IFFT image in the bottom left-hand inset clearly demonstrates the result. (f) The EDX image of the as-grown $Mo_{1-x}W_xSe_2$ alloys. This image shows the $Mo_{1-x}W_xSe_2$ alloys with the different stoichiometric ratio of Mo and W.

A_{1g} and $E_{2g}{}^1$ modes of $Mo_{1-x}W_xSe_2$ samples grown on the three different substrates have negligible differences in their peak positions. AFM is the most effective means to identify the number of layers of materials and study the surface structures of samples. The AFM image in Fig. 1(d) shows the thickness of the as-grown $Mo_{1-x}W_xSe_2$ alloy is about 0.9 nm, which indicates that the as-grown $Mo_{1-x}W_xSe_2$ alloy is a monolayer. The insetimagewithhomogeneouscolorcontrastinFig.1(d)indicatesthat the as-grown sample has a flat and uniform surface. TEM characterization technique is a powerful tool to study the crystal structures and composition information of 2D materials[33]. The low-resolution TEM image in the bottom left-hand panel of Fig. 1(e) clearly shows that the $Mo_{1-x}W_xSe_2$ sample on the copper grid meshes with the triangular shape. The sample inside the blue rectangle is chosen for element mapping and HRTEM (high-resolution transmission electron microscopy). The Mo, W, Se element mapping images in the bottom left-hand panel of Fig. 1(e) show the as-grown $Mo_{1-x}W_xSe_2$ alloys

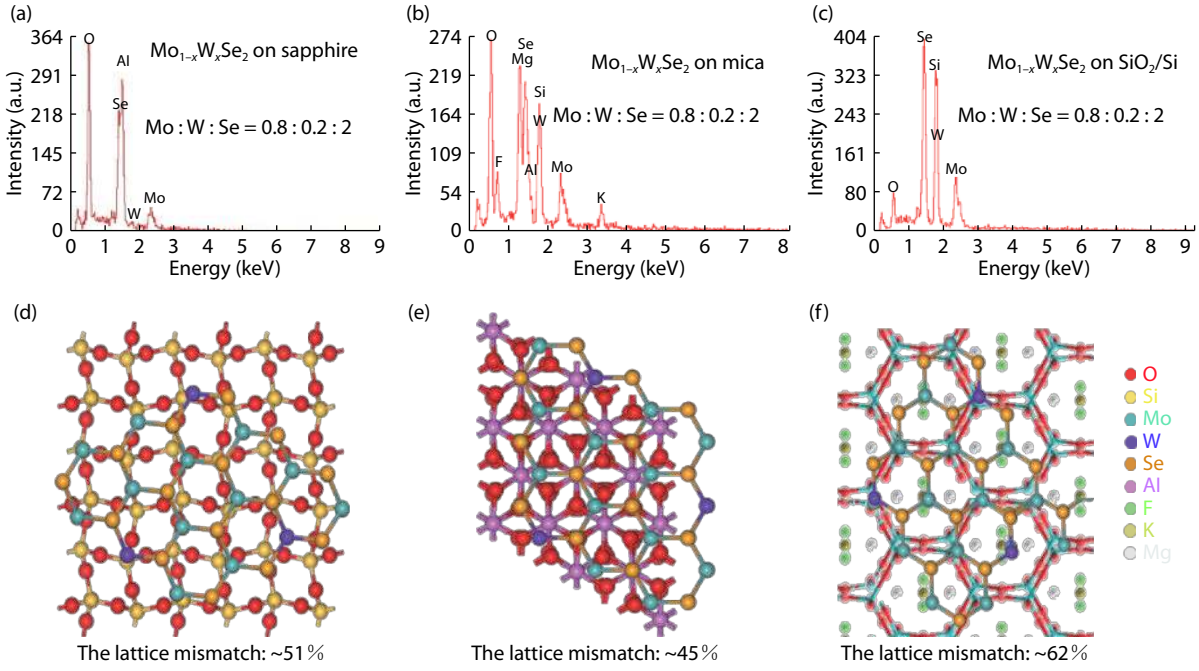

Fig. 2. (Color online) The EDX and lattice mismatch images of as-grown samples on different substrates. (a–c) show the EDX images of $Mo_{0.8}W_{0.2}Se_2$ alloys grown on SiO_2/Si, sapphire, and mica, respectively. (d–f) show the lattice mismatch images of $Mo_{1-x}W_xSe_2$ alloys on mica, SiO_2/Si, sapphire, respectively. The lattice mismatches of $Mo_{1-x}W_xSe_2$ alloys with SiO_2/Si, sapphire, and mica are about 51 %, 45 %, and 52 %, respectively.

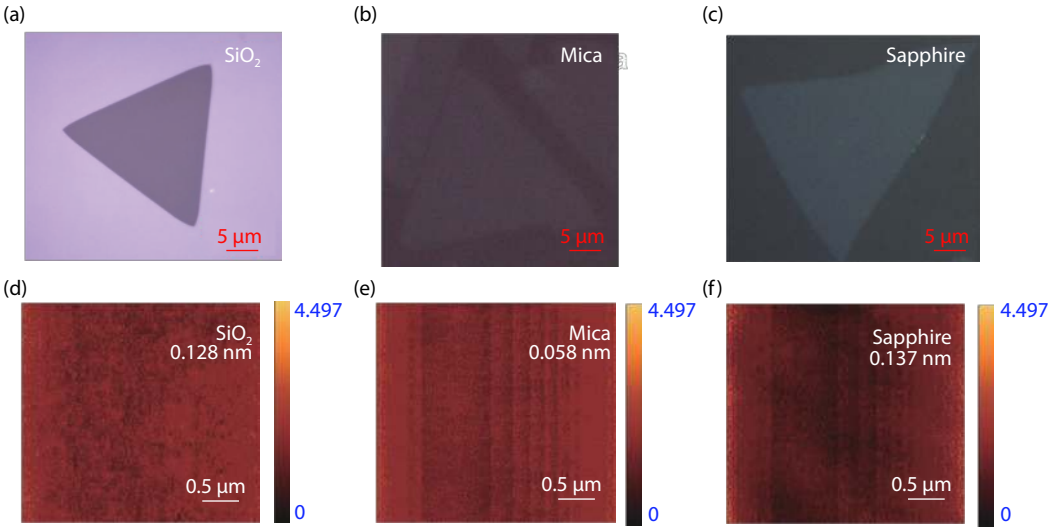

Fig. 3. (Color online) The optical images of the as-grown $Mo_{1-x}W_xSe_2$ on different substrates and the corresponding AFM images. The optical images of $Mo_{1-x}W_xSe_2$ alloys grown on (a) SiO_2/Si substrate, (b) mica substrate, (c) sapphire substrate. The scale bar is 5 μm. (d–f) show the corresponding AFM images of the SiO_2/Si, mica and sapphire, respectively. The RMS of the as-used SiO_2/Si, mica and sapphire is 0.128, 0.058, and 0.137 nm, respectively. The scale bar is 0.5 μm.

contain the Mo, W and Se atoms and indicate the uniform distribution of Mo, W, and Se atoms in the samples. The HRTEM image in the top view of Fig. 1(e) shows the clear atomic structure of as-grown $Mo_{1-x}W_xSe_2$ alloys. The lattice constant of the $Mo_{1-x}W_xSe_2$ alloy is 0.285 nm, which is between the lattice constant of $MoSe_2$ (0.28 nm)[34] and WSe_2 (0.33 nm)[35]. The top right inset of HRTEM image shows the corresponding selected area electron diffraction pattern (SAED), which demonstrates that the as-grown $Mo_{1-x}W_xSe_2$ samples have hexagon structure with good crystallinity. This result is further confirmed with the IFFT image in the bottom left-hand panel inset. There is only one set of diffraction pattern in the SAED image. The SAED image and Mo, W, Se element mapping images demonstrate the as-grown samples are $Mo_{1-x}W_xSe_2$ alloys rather than the heterostructures and binary counterparts. The energy dispersive X-ray spectroscopy (EDX) can be used to measure the relative content of the elements of materials. Fig. 1(f) shows the EDX image of $Mo_{1-x}W_xSe_2$ alloys with different stoichiometric ratio of Mo and W. The stoichiometric ratio of Mo and W changes from 0.1 : 0.9 to 0.9 : 0.1. The stoichiometric ratio of Mo and W changes from the mixture ratio of WO_3 and MoO_3 powders used as the precursors in the CVD method.

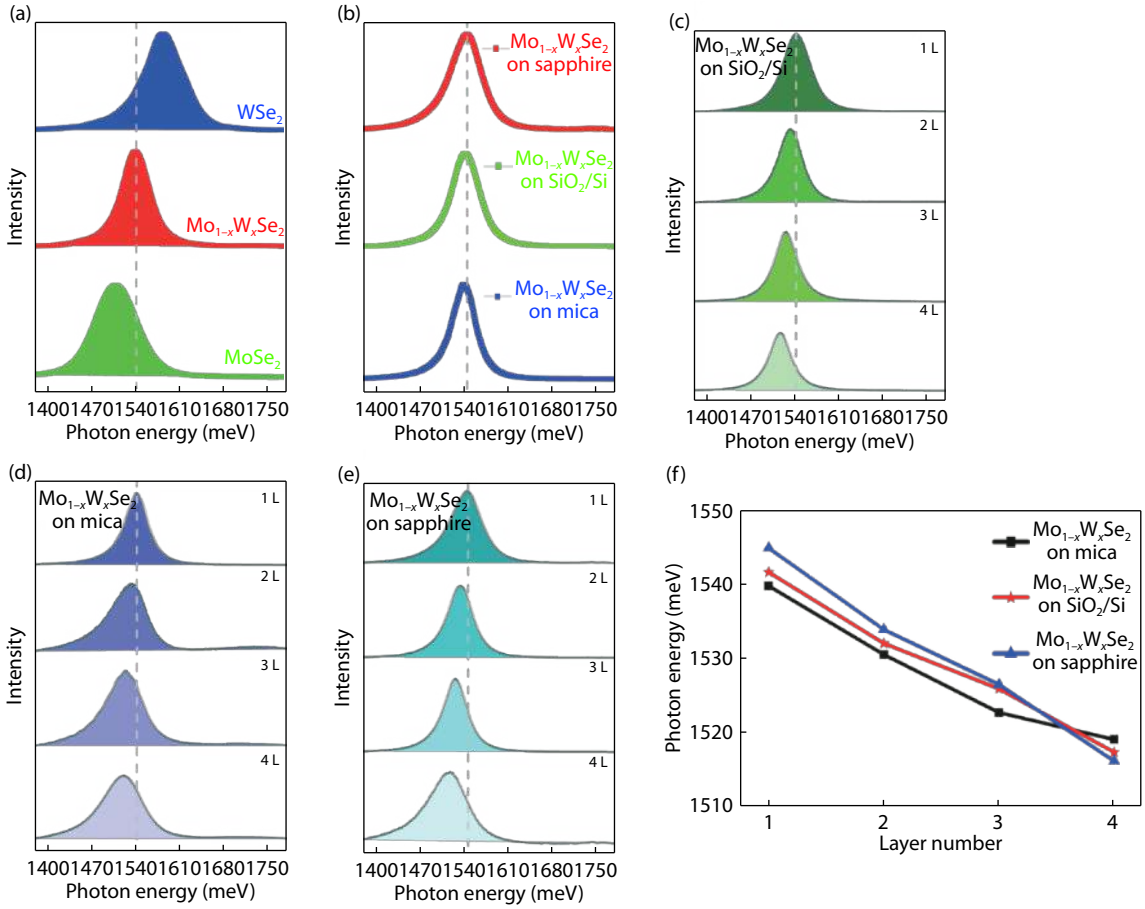

Fig. 4. (Color online) The PL characterization of the as-grown $Mo_{1-x}W_xSe_2$ alloys. (a) The PL image of the WSe_2, $Mo_{1-x}W_xSe_2$ and $MoSe_2$ grown on SiO_2/Si substrates. (b) The PL image of monolayer $Mo_{1-x}W_xSe_2$ alloys grown on SiO_2/Si, mica and sapphire. (c), (d) and (e) show the PL spectra of $Mo_{1-x}W_xSe_2$ alloys with different layers on sapphire, mica and SiO_2/Si, respectively. The dashed lines in (c–e) help clearly to distinguish the variation tendency of the bandgaps over the thickness (f) Thickness-dependent PL spectra of $Mo_{1-x}W_xSe_2$ alloys on SiO_2/Si, mica and sapphire substrates.

Figs. 2(a)–2(c) show the EDX image of $Mo_{0.8}W_{0.2}Se_2$ alloys on SiO_2/Si, sapphire and mica, respectively. These images show that the substrates have no effect on the stoichiometric ratio of the $Mo_{0.8}W_{0.2}Se_2$ alloys. Figs. 2(d)–2(f) show the lattice mismatch images of $Mo_{1-x}W_xSe_2$ alloys on mica, SiO_2/Si, and sapphire, respectively. The lattice mismatches of $Mo_{1-x}W_xSe_2$ alloys with SiO_2/Si, sapphire, and mica are about 51 %, 45 % and 52 %, respectively. Figs. 3(a)–3(c) show the optical images observed by the optical microscopy of $Mo_{1-x}W_xSe_2$ alloys grown on SiO_2/Si, mica, sapphire substrates, respectively. Optical microscopy is the simplest and most effective method to characterize the layered materials. The layer number of the materials can be first identified by the optical microscope. Figs. 3(d)–3(f) show the AFM images of the SiO_2/Si, mica, and sapphire, respectively. The root-mean-square (RMS) of the roughness of as-used SiO_2/Si, mica and sapphire is 0.128, 0.058, and 0.137 nm, respectively. Thus, mica can provide the smoothest surface among the three substrates for material synthesis.

PL spectroscopy is a direct method to characterize the optical bandgaps of 2D materials. Fig. 4(a) shows the PL spectra of WSe_2, $Mo_{1-x}W_xSe_2$ and $MoSe_2$ on SiO_2/Si substrates. The PL spectrum of $Mo_{1-x}W_xSe_2$ located at 1543 meV is in the range between that of WSe_2 located at 1592 meV and $MoSe_2$ located at 1510 meV. This result further demonstrates the as-grown samples are alloys. Fig. 4(b) show the PL spectra of monolayer $Mo_{1-x}W_xSe_2$ alloys grown on SiO_2/Si, mica and sapphire substrates. The changes of PL spectra of $Mo_{1-x}W_xSe_2$ alloys on these three substrates are merely about several meV, which demonstrates that the substrates have negligible effects on the optical bandgaps of as-grown $Mo_{1-x}W_xSe_2$ alloys. This finding provides an instructive idea for the choice of substrates to grow the alloys by CVD method. Figs. 4(c)–4(e) show the PL spectra of $Mo_{1-x}W_xSe_2$ alloys with different layers on sapphire, mica and SiO_2/Si, respectively. The bandgaps redshift as the layer numbers of the samples increase, which demonstrates that the interlayer coupling effects related to the layer numbers have large effects on the optical bandgaps of $Mo_{1-x}W_xSe_2$ alloys. Fig. 4(f) show the corresponding thickness-dependent PL spectra of $Mo_{1-x}W_xSe_2$ alloys on SiO_2/Si, mica and sapphire from Figs. 4(c)–4(e). The peak position variations of $Mo_{1-x}W_xSe_2$ alloys with different thickness are larger than the $Mo_{1-x}W_xSe_2$ alloys growing on different three substrates. Our results demonstrate that the interlayer coupling effect on the optical bandgaps of $Mo_{1-x}W_xSe_2$ alloys is greater than the substrates effect.

3. Conclusion

In conclusion, $Mo_{1-x}W_xSe_2$ films are synthesized on sapphire, mica and SiO_2/Si substrates by the CVD method. The AFM, Raman and PL characterization techniques are used to ascertain the monolayer nature of the as-grown samples. The EDX spectra show the adjustable stoichiometric ratio of the 2D alloy materials synthesized by the CVD method. The TEM res-

ults indicate the high quality and homogeneity of the as-grown samples. The Raman and AFM results show the roughness of the substrates have a negligible effect on the E_{2g}^1 of the $Mo_{1-x}W_xSe_2$ alloys. The PL results indicate that the substrates have negligible effects on the bandgaps of $Mo_{1-x}W_xSe_2$ alloys and also show that the interlayer coupling effect related to the layer numbers on the optical bandgaps of $Mo_{1-x}W_xSe_2$ alloys is larger than the substrates effect. These findings prove a new way for the future study of the growth dynamics and physical properties of two-dimensional materials.

Acknowledgements

This work was supported by the National Natural Science Foundation of China (Nos. 11504111, 61574060), the Projects of Science and Technology Commission of Shanghai Municipality (Nos. 15JC1401800, 14DZ2260800), the Program for Professor of Special Appointment (Eastern Scholar), the Shanghai Rising-Star Program (No. 17QA1401400), the Young Elite Scientists Sponsorship (YESS) Program by CAST, and the Fundamental Research Funds for the Central Universities.

Appendix A

Synthesis of $Mo_{1-x}W_xSe_2$ films: $Mo_{1-x}W_xSe_2$ films are synthesized in a CVD furnace (Thermo Scientific Lindberg/Blue M Moldatherm) with a one-inch diameter quartz tube. Se powders (99.99 %, Sigma-Aldrich) put in a quartz boat are placed upstream at the edge of the furnace. The mixture MoO_3 powders (99.9 %, Sigma-Aldrich) and WO_3 powders (99.9 %, Sigma-Aldrich) are put in the center of the face-to-face substrates. The substrates (mica, sapphire, 300 nm SiO_2/Si) with a mixture of MoO_3 and WO_3 powders are put on a quartz sheet and are then placed in the heating center. The velocity of carrier gas argon (Ar) is kept for 80 to 100 standard cubic centimeters per minute (sccm) after purifying the system with 200 sccm Ar for 30 min. The furnace is heated to 900 °C with a heating rate of 20 °C/min and keeps at 900 °C for 15 min. After the growth process is completed, the furnace is cooled to room temperature.

Characterization: Optical images are obtained by using an optical microscope (OLYMPUS BX41M-LED). Raman spectra and PL spectra are tested by using a Raman spectroscopy (Horiba, LabRAM HR-800) with a laser excitation wavelength of 532 nm. The grating for Raman spectra is 1800 l/mm and for PL spectra is 300 l/mm. The laser beam is focused on the samples to a diameter of ~ 2 μm by a × 50 objective. The laser power is adjusted at a power of ~ 3.7 mW to minimize the laser-induced thermal effect. EDX characterization is carried out on an FEI XL30 ESEM facility with the acceleration voltage of 10 kV. The surface morphology and layer numbers are characterized by AFM technique (MicroNano D-5A). TEM samples are prepared by using a PMMA assisted transfer technology. The TEM images are recorded at 200 kV on a JEOL 2100F.

References

[1] Zhang G, Huang S, Chaves A, et al. Infrared fingerprints of few-layer black phosphorus. Nat Commun, 2017, 8, 14071
[2] Mogi M, Kawamura M, Yoshimi R, et al. A magnetic heterostructure of topological insulators as a candidate for an axion insulator. Nat Mater, 2017, 16(5), 516
[3] Zhang Y, Chang T R, Zhou B, et al. Direct observation of the transition from indirect to direct bandgap in atomically thin epitaxial $MoSe_2$. Nat Nanotechnol, 2014, 9(2), 111
[4] Bertolazzi S, Gobbi M, Zhao Y, et al. Molecular chemistry approaches for tuning the properties of two-dimensional transition metal dichalcogenides. Chem Soc Rev, 2018, 47(17), 6845
[5] Manimunda P, Nakanishi Y, Jaques Y M, et al. Nanoscale deformation and friction characteristics of atomically thin WSe_2 and heterostructure using nanoscratch and Raman spectroscopy. 2D Mater, 2017, 4(4), 045005
[6] Wang C, Wu X, Ma Y, et al. Metallic few-layered VSe_2 nanosheets: high two-dimensional conductivity for flexible in-plane solid-state supercapacitors. J Mater Chem A, 2018, 6(18), 8299
[7] Xiao S, Xiao P, Zhang X, et al. Atomic-layer soft plasma etching of MoS_2. Sci Rep, 2016, 6, 19945
[8] Zhang X, Nan H, Xiao S, et al. Shape-uniform, high-quality monolayered MoS_2 crystals for gate-tunable photoluminescence. ACS Appl Mater Inter, 2017, 9(48), 42121
[9] Novoselov K S, Geim A K, Morozov S V, et al. Electric field effect in atomically thin carbon flims. Science, 2004, 306(5686), 666
[10] Zheng Z, Yao J, Yang G. Centimeter-scale deposition of $Mo_{0.5}W_{0.5}Se_2$ alloy film for high-performance photodetectors on versatile substrates. ACS Appl Mater Inter, 2017, 9(17), 14920
[11] Liu J, Zhong M, Liu X, et al. Two-dimensional plumbum-doped tin diselenide monolayer transistor with high on/off ratio. Nanotech, 2018, 29(47), 474002
[12] Zhou W, Zou X, Najmaei S, et al. Intrinsic structural defects in monolayer molybdenum disulfide. Nano Lett, 2013, 13(6), 2615
[13] Yao J, Zheng Z, Yang G. Promoting the performance of layered-material photodetectors by alloy engineering. ACS Appl Mater Inte, 2016, 8(20), 12915
[14] Lu C P, Li G, Mao J, et al. Bandgap, mid-gap states, and gating effects in MoS_2. Nano Lett, 2014, 14(8), 4628
[15] Kang J, Tongay S, Li J, et al. Monolayer semiconducting transition metal dichalcogenide alloys: Stability and band bowing. J Appl Phys, 2013, 113(14), 143703
[16] Peng Q, De S. Tunable band gaps of mono-layer hexagonal BNC heterostructures. Physica E, 2012, 44(7/8), 1662
[17] Ye J, Niu B, Li Y, et al. Exciton valley dynamics in monolayer $Mo_{1-x}W_xSe_2$ ($x = 0, 0.5, 1$). Appl Phys Lett, 2017, 111(15), 152106
[18] Zhang C, Kc S, Nie Y, et al. Charge mediated reversible metal–insulator transition in monolayer $MoTe_2$ and $W_xMo_{1-x}Te_2$ alloy. ACS Nano, 2016, 10(8), 7370
[19] Livneh T, Dumcenco D O, Pinkas I. Determining alloy composition in $Mo_xW_{(1-x)}S_2$ from low wavenumber Raman spectroscopy. J Raman Spectrosc, 2017, 48(5), 773
[20] Li H, Zhang Q, Duan X, et al. Lateral growth of composition graded atomic layer $MoS_{(2(1-x))}Se_{(2x)}$ nanosheets. J Am Chem Soc, 2015, 137(16), 5284
[21] Liu J, Liu X, Chen Z, et al. Tunable Schottky barrier width and enormously enhanced photoresponsivity in Sb doped SnS_2 monolayer. Nano Res, 2018, 12(2), 463
[22] Li H, Duan X, Wu X, et al. Growth of alloy $MoS_{(2x)}Se_{2(1-x)}$ nanosheets with fully tunable chemical compositions and optical properties. J Am Chem Soc, 2014, 136(10), 3756
[23] Duan X, Wang C, Fan Z, et al. Synthesis of $WS_{2x}Se_{2-2x}$ alloy nanosheets with composition-tunable electronic properties. Nano Lett, 2016, 16(1), 264
[24] Chen Y, Dumcenco D O, Zhu Y, et al. Composition-dependent Raman modes of $Mo_{(1-x)}W_{(x)}S_2$ monolayer alloys. Nanoscale, 2014, 6(5), 2833
[25] Dumcenco D O, Kobayashi H , Liu Z, et al. Visualization and quantification of transition metal atomic mixing in $Mo_{1-x}W_xSe_2$ single layers. Nat Commun, 2013, 4, 1351
[26] Song J G, Ryu G H, Lee S J, et al. Controllable synthesis of molybdenum tungsten disulfide alloy for vertically composition-controlled multilayer. Nat Commun, 2015, 6, 7817

[27] Dumcenco D O, Chen K Y, Wang Y P, et al. Raman study of 2H-$Mo_{1-x}W_xS_2$ layered mixed crystals. J Alloy Compd, 2010, 506(2), 940

[28] Zhang X, Xiao S, Shi L, et al. Large-size $Mo_{1-x}W_xS_2$ and $Mo_{1-x}W_xS_2$ (x = 0–0.5) monolayers by confined-space chemical vapor deposition. Appl Surf Sci, 2018, 457, 591

[29] Ke T Y, Hsu H P, Wang Y P, et al. Temperature dependent piezoreflectance study of $Mo_{1-x}W_xSe_2$ layered crystals. J Appl Phys, 2015, 118(21), 215704

[30] Yarali M, Brahmi H, Yan Z, et al. Effect of metal doping and vacancies on the thermal conductivity of monolayer molybdenum diselenide. ACS Appl Mater Inter, 2018, 10(5), 4921

[31] Xu H, Wu X, Li X, et al. Properties of graphene-metal contacts probed by Raman spectroscopy. Carbon, 2018, 127, 491

[32] Liang F, Xu H, Wu X, et al. Raman spectroscopy characterization of two-dimensional materials. Chin Phys B, 2018, 27(3), 037802

[33] Luo C, Wang C, Wu X, et al. In situ transmission electron microscopy characterization and manipulation of two-dimensional layered materials beyond graphene. Small, 2017, 13(35), 1604259

[34] Xia J, Huang X, Liu L Z, et al. CVD synthesis of large-area, highly crystalline $MoSe_2$ atomic layers on diverse substrates and application to photodetectors. Nanoscale, 2014, 6(15), 8949

[35] Huang J, Yang L, Liu D, et al. Large-area synthesis of monolayer WSe_2 on a SiO_2/Si substrate and its device applications. Nanoscale, 2015, 7(9), 4193